FACTA UNIVERSITATIS
Series: **Mechanical Engineering**
https://doi.org/10.22190/FUME201225014S

Original scientific paper

MODELING OF TITANIUM ALLOYS PLASTIC FLOW IN LINEAR FRICTION WELDING

Vladimir A. Skripnyak, Kristina Iokhim, Evgeniya Skripnyak, Vladimir V. Skripnyak

National Research Tomsk State University, Russia

Abstract. *The article presents the results of the analysis of the plastic flow of titanium alloys in the process of the Linear Friction Welding (LFW). LFW is a high-tech process for joining critical structural elements of aerospace engineering from light and high-temperature alloys. Experimental studies of LFW modes of such alloys are expensive and technically difficult. Numerical simulation was carried out for understanding the physics of the LFW process and the formation laws of a strong welded joint of titanium alloys. Simulation by the SPH method was performed using the LS DYNA software package (ANSYS WB 15.2) and the developed module for the constitutive equation. The new coupled thermomechanical 3D model of LFW process for joining structural elements from alpha and alpha + beta titanium alloys was proposed. It was shown that the formation of a welded joint occurs in a complex and unsteady stress-strain state. In the near-surface layers of the bodies being welded, titanium alloys can be deformed in the mode of severe plastic deformation. A deviation of the symmetry plane of the plastic deformation zone from the initial position of the contact plane of the bodies being welded occurs during a process of LFW. Extrusion of material from the welded joint zone in the transverse direction with respect to the movement of bodies is caused by a pressure gradient and a decrease in the alloy flow stress due to heating. The hcp-bcc phase transition of titanium alloys upon heating in the LFW process necessitates an increase in the cyclic loading time to obtain a welded joint.*

Key words: *Linear friction welding, 3D numerical simulation, SPH simulation, Titanium alloys, Mechanical response*

1. INTRODUCTION

Friction welding is a technology that allows two or more identical or dissimilar materials with different melting points to be welded using the heat generated by friction,

Received December 25, 2020 / Accepted February 03, 2021
Corresponding author: Vladimir V. Skripnyak
National Research Tomsk State University, 36 Lenin Avenue, Tomsk, 634050, Russia
E-mail: skrp2012@yandex.ru

and also the mechanical mixing of the materials at the joint surface. Friction welding makes it possible to obtain strong welded joints of various alloys containing elements such as titanium, aluminum, magnesium, etc., as well as to obtain welded joints of steels [1-4].

In modern engineering practice, two modifications of friction welding technology are used Linear Friction Welding (LFW) and Friction stir welding (FSW) [1-11].

LFW makes it possible to obtain strong joining of materials at the contact interface plane of moved bodies through the heat generation at friction and material particle transport between contacting bodies [5-7]. LFW is a manufacturing process used primarily within the aviation industry, where high integrity welds are required in aero-engine production [5]. This technology is used for welding critical parts of power equipment, such as bladed-disk (blisk) of turbines [7].

FSW is one method of solid-state joining titanium and its alloys that can prevent the mechanical properties of titanium welded joints from deteriorating by other welding processes [1, 2, 12-14].

In the last decade, experimental and theoretical studies of the physical processes underlying friction welding have been carried out.

It was found that during friction welding there is a significant heating of the material in the zone of formation of the weld, which contributes to the development of large plastic deformations. In the heating zone, phase transformations can occur in metals and alloys, for example, in titanium alloys [1, 5, 6]. Therefore, the selection of friction welding modes for titanium alloys with different chemical and phase compositions is a complex engineering and technological problem [12−16].

The results obtained by Popov and coworkers indicate that the adhesive contact of flat bodies can clearly depend on the macroscopic shape of the contact zone [17]. Therefore, the shape of the contact zone of interacting bodies formed as a result of LFW can influence the strength characteristics of the welded joint [7].

The material structure and the presence of damage in it after plastic deformation have the decisive importance to the strength of the weld seam obtained by friction welding. Loss of the adhesion between the tool and the material will inevitably lead to damage nucleation and decrease in the strength of the weld.

The results of experimental studies of friction welding processes have become the basis for validating the methods for modeling physical processes that underlie these technologies [1-5]. Various types of numerical methods were used for numerical simulation of LFW and FSW processes [15-24].

Balokhonov and coworkers numerically studied the localization of plastic deformation of an aluminum alloy in a welded joint obtained by the FSW method [18]. It was shown that different zones in welding joint demonstrate distinct deformation response to loading due to peculiar combinations of the grain geometry and crystallographic texture.

Smolin and coworkers showed the possibility of predicting the parameters of the friction stir welding process based on numerical simulation of the process using the movable cellular automaton method (MCA) [19]. It was shown by numerical modeling, that the ratio of the rotation speed to the speed of advancement of the FSW tool significantly affects the quality of the joint and the formation of microcracks and micropores in the welded joint of plates made of duralumin alloy D−16. It was also shown that the geometric parameters of the tool pins affect the movement of the plasticized

material in the zone of formation of the weld. Modification of the geometric parameters and the shape of the pins make it possible to improved mechanical properties of the welded joint.

Tarlakovsky and coworkers applied the numerical SPH technique to study the FSW process. It has been shown that the Smoothed−Particle Hydrodynamics (SPH) method allows one to describe the process of mixing materials on a scale that depends only on the number of particles [23-24]. The SPH method makes it possible to use a thermodynamic model to predict the generation of heat as a result of the interaction of the surface with the tool pin and due to the dissipation of the energy of work stresses on plastic deformations.

Yang and coworkers applied the numerical modeling of the FSW to predict microstructural transformations in aluminum alloy 6061 in heat-affected zones: the weld nugget zone (WNZ), the thermal-mechanical-affected zone (TMAZ), the heat-affected zone (HAZ), and the base-material zone (BZ) [21]. It has been shown that the computational FSW model cannot fully simulate a real welding situation. Therefore, the theoretical predictions obtained with the COMSOL Multi-Physics software differ from the experimental data.

Fall and coworkers showed that the size and morphology of grains observed in various zones (BZ, HAZ and TMAZ) of FSW Ti-6Al-4V titanium alloy are distinctly different as revealed by the microstructure analysis. The obtained experimental results confirm the significant influence of structural transformations in the grain structure of titanium alloy during friction welding on the strength characteristics of the welded joint.

Chauhan and coworkers showed the possibility of using the coupled Euler-Lagrange method and the use of the Johnson-Cook constitutive equation in the numerical simulation of FSW of plates made of AA 6061-T6 aluminum alloy. The results of modeling the FSW mode, taking into account the physical and mechanical response of the alloy in the process of plastic flow at high strain rate, showed that the tensile strength of the welded joint is directly proportional to the effective plastic deformation. Welding efficiency 90% and 65% are found for effective plastic deformation 230 and 60, respectively. These results indicate the need for an adequate description of the mechanical behavior of friction welded materials in the ranges of temperature, strain rates, and equivalent plastic strains, which are realized during friction welding.

Despite efforts to create a method for modeling physical mechanisms in friction welding technologies, there is still no complete understanding of their regularities and determining factors.

In this article, the processes of deformation, damage and heating of titanium alloys in the process of LFW were studies by SPH method of three-dimensional computer simulation. The wide-range constitutive model developed by authors was used for describing the mechanical behavior of the alpha and alpha+beta titanium alloys [25−29]. This model is used to describe the plastic flow of titanium alloys, taking into account the effects of its localization, strain hardening, thermal softening, strain rate sensitivity of the flow stress, and patterns of damage nucleation and growth.

2. MODEL AND COMPUTATIONAL DETAILS

2.1. Model of LFW

In this work, the coupled 3D computational model of the LFW thermomechanical process was developed on the base of LS DYNA software (ANSYS WB 15.2). The model was applied for LFW simulation of the friction pair deformable blocks (Fig. 1). The blocks dimensions for the SPH model were: a= 2.5 mm; b= 5 mm; L_0= 2.5 mm; d = b/2.

A system of particles was generated in blocks with an initial smoothing length equals to 0.1 mm. Particles with the same initial density had the same initial volume. The SPH method with variable smoothing length was used for numerical simulation by LS-Dyna/WB ANSYS 15.2 software. The lower block moved back and forth at a velocity that changed as $V_1(t) = V_0 \sin(\omega t)$. The friction welding process was simulated at a frequency of speed change of 50 Hz. The ranges of displacement amplitudes and frequencies of changing velocity were chosen in accordance with the parameters realized in the McAndrew experiments on LFW of Ti-6Al-4V blocks [30].

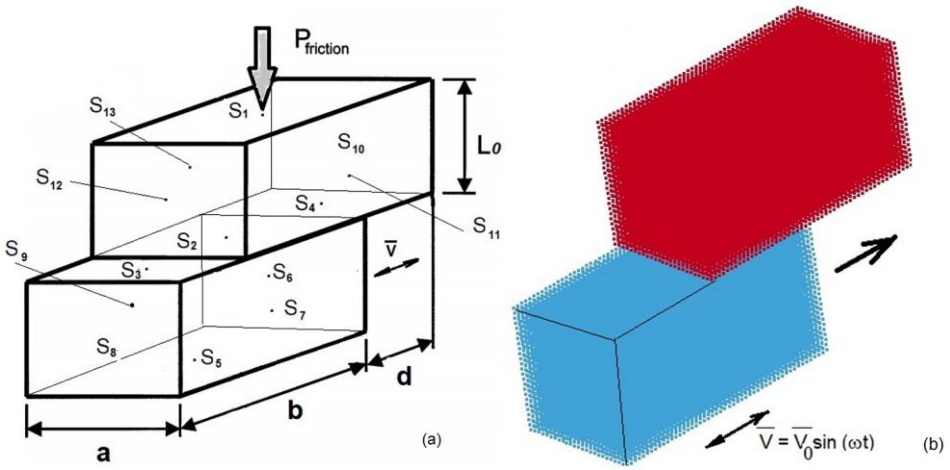

Fig. 1 Scheme of LFW is shown in (a), SPH model of blocks in contact at LFW is presented in (b)

The computational model uses the theoretical basis of continuum damage mechanics. The system of equations includes:

- conservation equations Eq. (1) − Eq. (3),
- kinematic relations Eq. (4) − Eq. (5),
- constitutive relations Eq. (6) − Eq. (7),
- equation of state (EOS) Eq. (8) − Eq. (10),
- relaxation equation for the deviatoric stress tensor Eq. (11),
- decomposition of strain rate into elastic and inelastic components Eq. (12),
- equations for inelastic strain rates Eq. (13) – Eq. (15).

$$\frac{d\boldsymbol{\rho}}{dt} = \boldsymbol{\rho}\frac{\partial u_i}{\partial x_i} \tag{1}$$

$$\frac{\partial \boldsymbol{\sigma}_{ij}}{\partial x_j} = \boldsymbol{\rho}\frac{du_i}{dt} \tag{2}$$

$$\boldsymbol{\rho}\frac{dE}{dt} = \boldsymbol{\sigma}_{ij}\,\boldsymbol{\varepsilon}'_{ij} \tag{3}$$

$$\boldsymbol{\varepsilon}'_{ij} = (1/2)[\partial u_i / \partial x_j + \partial u_j / \partial x_i) \tag{4}$$

$$\boldsymbol{\omega}'_{ij} = (1/2)[\partial u_i / \partial x_j - \partial u_j / \partial x_i) \tag{5}$$

$$\boldsymbol{\sigma}_{ij} = \boldsymbol{\sigma}_{ij}^{(m)}\boldsymbol{\varphi}(f) \tag{6}$$

$$\boldsymbol{\sigma}_{ij}^{(m)} = -p^{(m)}\,\boldsymbol{\delta}_{ij} + S_{ij}^{(m)} \tag{7}$$

$$p^{(m)} = p_x^{(m)}(\boldsymbol{\rho}) + \Gamma(\boldsymbol{\rho})\boldsymbol{\rho}E_T \tag{8}$$

$$E = E_x + E_T\ ,\ E_T = C_pT\ ,\ E_x = \int_{V_0}^{V} p_x^{(m)}\,dV \tag{9}$$

$$p_x^{(m)} = \frac{3}{2}B_0 \cdot ((\boldsymbol{\rho}_0/\boldsymbol{\rho})^{-7/3} - (\boldsymbol{\rho}_0/\boldsymbol{\rho})^{-5/3})[1 - \frac{3}{4}(4 - B_1)\cdot((\boldsymbol{\rho}_0/\boldsymbol{\rho})^{-2/3} - 1)] \tag{10}$$

$$DS_{ij}^{(m)}/Dt = 2G(\dot{\varepsilon}_{ij}^{e} - \delta_{ij}\dot{\varepsilon}_{kk}^{e}/3) \tag{11}$$

$$\boldsymbol{\varepsilon}'_{ij} = \dot{\boldsymbol{\varepsilon}}_{ij}^{e} + \dot{\boldsymbol{\varepsilon}}_{ij}^{p} \tag{12}$$

$$\dot{\boldsymbol{\varepsilon}}_{ij}^{p} = \dot{e}_{ij}^{p} + \boldsymbol{\delta}_{ij}\dot{\boldsymbol{\varepsilon}}_{kk}^{p}/3 \tag{13}$$

$$\dot{e}_{ij}^{p} = \boldsymbol{\lambda}\partial\Phi/\partial\boldsymbol{\sigma}_{ij} \tag{14}$$

$$\dot{\boldsymbol{\varepsilon}}_{kk}^{p} = \dot{f}_{growth}/(1-f) \tag{15}$$

where $\boldsymbol{\rho}$ is the mass density; u_i is the component of the particle velocity vector; x_i are Cartesian coordinates, i = 1,2,3; t is the time; $\boldsymbol{\sigma}_{ij}$ are components of the Cauchy stress tensor; $p^{(m)}$ is the pressure in a condensed part of material; S_{ij} components of the deviatoric stress tensor; $\boldsymbol{\delta}_{ij}$ is the Kronecker delta; E is the specific internal energy; E_T is the thermal part of specific internal energy; E_x is the "cold" contribution to specific internal energy; $V = 1/\boldsymbol{\rho}$ is the specific volume; $\boldsymbol{\varepsilon}'_{ij}$, and $\boldsymbol{\omega}'_{ij}$ are components of the strain rate tensor and the bending-torsion rate tensor, respectively; superscript m means that the parameters refer to the undamaged part of the material; superscript e means the elastic part of strain rate tensor; superscript p means the inelastic part of strain rate tensor; $\boldsymbol{\varphi}(f)$ is a function that links the effective stresses in the damaged material with the stresses in the

undamaged part of the material; $\mathbf{\Gamma(\rho)} = \gamma_R(\rho_R/\rho)+0.5[1 - (\rho_R/\rho)]^2$ is the Grüneisen function describing by the Kerley's relation; ρ_0 is the initial mass density of condensed phase of alloy; γ_R, ρ_R, B_0, B_1 are constants of undamaged part of material; C_p is the specific heat capacity; T is temperature in absolute scale; D(·)/Dt is the Jaumann's derivative; G is the shear modulus; $\dot{f}_{growth}$ is the damage growth rate; f is the damage parameter corresponding to the specific volume of voids in material; λ is the plastic multiplier derived from the consistency condition $d\Phi/dt = 0$; Φ is the plastic potential.

Experimental studies of the LFW process have shown that materials in the welding zone are deformed not only at high temperatures, but also at high hydrostatic pressures [5, 6, 10]. Therefore, it is important to use a nonlinear equation of state, which describes the compressibility of titanium alloys in wide ranges of temperature and pressure for obtaining adequate results of modeling the processes of LFW.

The pressure was calculated by the Mie-Grüneisen EOS model. The Grüneisen function $\mathbf{\Gamma(\rho)}$ was determined with the following values of the constants: γ_R =1.184, ρ_R = 4.5018 10^3 kg/m^3, ρ_0 =4.5405 10^3 kg/m^3 for alpha titanium, and γ_R =1.25, ρ_R = 4.5018 10^3 kg/m^3, ρ_0 =4.4588 10^3 kg/m^3 for Ti-6Al-4V alloy.

The Birch-Murnaghan equation was used to describe the zero-Kelvin isotherms $p_x^{(m)}$. The bulk modulus and its pressure derivative were taken equal to B_0 = 111.0 GPa, B_1 = 3.48 for alpha titanium and B_0 = 111.0 GPa, B_1 = 3.58 for Ti-6Al-4V, respectively. The equation of state was calibrated to pressures of 125 GPa for alpha titanium and Ti-6Al-4V alloy. The plastic potential Φ was described using the Gurson-Tvergaard-Needleman model (GTN) [29-33]. The function $\varphi(f)$ takes the form $(1-f)$ for pressure and is implicitly defined for the deviatoric stress tensor [31, 32].

2.2. Model of mechanical behavior titanium alloys

Heat is released in plastically deformable layers of materials arising in the friction zone of moving blocks. The actual contact area increases due to wear and thermal softening of the materials.

The temperature rise associated with energy dissipation during plastic flow can be evaluated by Eq. (16) [33]:

$$T = T_0 + \int_0^{\varepsilon_{eq}^p} (\beta / \rho C_p)\sigma_{eq} d\varepsilon_{eq}^p \tag{16}$$

where $\beta \sim 0.9$ is parameter representing a fraction of plastic work converted into heat; $\sigma_{eq} = [(3/2)\ \sigma_{ij}\ \sigma_{ij} - (1/2)\ \sigma_{kk}\ \sigma_{kk}]^{1/2}$ is the equivalent stress; $d\varepsilon^p_{eq}$ is the increment of the equivalent plastic strain; $\varepsilon^p_{eq} = [(3/2)\ \varepsilon_{ij}\ \varepsilon_{ij} - (1/2)\ \varepsilon_{kk}\ \varepsilon_{kk}]^{1/2}$.

The specific heat capacity for alpha titanium alloys was calculated by the phenomenological relations within temperature range from 293 to 1115 K [34, 35]:

$$C_p = 248.389 + 1.53067T - 0.00245T^2 [J/kgK]\ at\ 0 < T < T_{\alpha\beta} = 1320\ K \tag{17}$$

The specific heat capacity for Ti6Al4V titanium was calculated using data [9]:

$$C_p = 375.4343 + 1.12061T - 0.00147T^2 + 7.10^{-7} T^3 [J/kgK]\ at\ 0 < T < T_{\alpha\beta} = 1373\ K \tag{18}$$

The heat affected zone (HAZ) expands into the volume of the contacting blocks during the process of their cyclic movement. The temperature distribution in the bodies to be welded must be determined taking into account the thermal conductivity. In this work, it was assumed that the most significant is conductive heat transfer.

Temperature history is calculated using the heat diffusion Eq. (19):

$$\rho C_p \partial T / \partial t = k(T)[\partial^2 T / \partial^2 x_1 + \partial^2 T / \partial^2 x_2 + \partial^2 T / \partial^2 x_3] \tag{19}$$

where k is the thermal conductivity coefficient.

The thermal conductivity coefficient was described by phenomenological Eq. (20):

$$k(T) = k_0 + k_1 T \tag{20}$$

where k_0, and k_1 are parameters of material.

Coefficients k_0 = 3.48568 W/(m K), and k_1 = 0.01077 W/(m K^2) were determined using experimental data for Ti-6Al-4V [8].

The temperature dependence of the shear modulus for titanium alloys was described by Eq. (21):

$$G(T) = 48.66 - 0.03223\,T \ \ [GPa]\,, (273K < T < 1200\,K) \tag{21}$$

The plastic flow stress $\boldsymbol{\sigma}_s$ was described by Eq. (22):

$$\begin{gathered} \boldsymbol{\sigma}_s = \boldsymbol{\sigma}_{s0} \exp\{C_1 \sqrt{(1 - T / T_m)}\} + C_2 \sqrt{1 - \exp\{-k_2 \boldsymbol{\varepsilon}_{ef}^p\}} \exp\{-C_3 T\} \exp\{C_4 T \ln(\dot{\boldsymbol{\varepsilon}}_{eq} / \dot{\boldsymbol{\varepsilon}}_{eq0})\} \\ \dot{\boldsymbol{\varepsilon}}_{eq} = [(2/3)\dot{\boldsymbol{\varepsilon}}_{ij} \dot{\boldsymbol{\varepsilon}}_{ij}]^{1/2} \\ \dot{\boldsymbol{\varepsilon}}_{eq0} = \boldsymbol{\gamma}_1 \exp\{-T / \boldsymbol{\gamma}_2\} + \boldsymbol{\gamma}_3 \\ \boldsymbol{\varepsilon}_{ef}^p = \int_0^t \dot{\boldsymbol{\varepsilon}}_{eq}^p dt \end{gathered} \tag{22}$$

where $\boldsymbol{\varepsilon}^p_{ef}$ is the effective plastic strain, and T_m is the melting temperature, $\boldsymbol{\sigma}_{s0}$, C_1, C_2, C_3, C_4, k_2, $\boldsymbol{\gamma}_1$, $\boldsymbol{\gamma}_2$, $\boldsymbol{\gamma}_3$ are coefficients of material.

The value of effective plastic strain $\boldsymbol{\varepsilon}^p_{ef}$ is the integral of stepwise increments of equivalent plastic strain for a period of time t. Material coefficients of some titanium alloys presented in Table 1.

Table 1 Model coefficients for titanium alloys

Coefficients of Eq. (22)	σ_{s0}, GPa	C_1	C_2, GPa	C_3, K^{-1}	C_4 ,K^{-1}	k_2	T_m, K
Ti-5Al-2.5Sn (Grade 6)	0.02	3.85	0.56	0.0016	0.00009	8.5	1875
Ti-6Al-4V (Grade 5)	0.041	3.4	0.84	0.0026	0.00009	8.5	1933
Alpha Ti (Grade 2)	0.04138	6.2	0.1843	0.000877	0.00004	8.5	1938

The values of coefficients γ_1= 2115.08615 s^{-1}, γ_2 =38.26589 K, and γ_3= 9.82388 10^{-5} s^{-1} were used to determine the normalizing parameter in Eq. (22) for titanium alloys.

2.3. Damage model

In this paper, numerical modeling of a titanium alloys was carried out taking into account the influence of the triaxiality stress state on the evolution of damage up to the ductile fracture.

The Lode parameter L and the triaxiality of stress state parameter η were determined by the relations [29]:

$$\begin{aligned} L &= \left(2\,\boldsymbol{\sigma}_{II} - \boldsymbol{\sigma}_{I} - \boldsymbol{\sigma}_{III}\right) / \left(\boldsymbol{\sigma}_{I} - \boldsymbol{\sigma}_{III}\right) \\ \boldsymbol{\eta} &= -p / \boldsymbol{\sigma}_{eq} = \sqrt{3}\boldsymbol{\sigma}_{I} / \sqrt{\boldsymbol{\sigma}_{II}} \end{aligned} \tag{23}$$

where $\boldsymbol{\sigma}_{ij}$ are the components of the Cauchy stress tensor, p = - $\boldsymbol{\sigma}_I/3$ is the pressure, $\boldsymbol{\sigma}_I=\boldsymbol{\sigma}_{kk}$, $\boldsymbol{\sigma}_{II}$ = (1/2) ($\boldsymbol{\sigma}_{ii}$ $\boldsymbol{\sigma}_{jj}$ - $\boldsymbol{\sigma}_{ij}$ $\boldsymbol{\sigma}_{ij}$), $\boldsymbol{\sigma}_{III}$ = $\boldsymbol{\sigma}_{11}\boldsymbol{\sigma}_{22}\boldsymbol{\sigma}_{33}+2\boldsymbol{\sigma}_{12}\boldsymbol{\sigma}_{23}\boldsymbol{\sigma}_{31} - \boldsymbol{\sigma}^2_{12}\boldsymbol{\sigma}_{33} - \boldsymbol{\sigma}^2_{23}\boldsymbol{\sigma}_{11} - \boldsymbol{\sigma}^2_{31}\boldsymbol{\sigma}_{22}$ are the first, the second and the third invariants of the Cauchy stress tensor, respectively.

The influence of damage on the flow stress was described by GTN model [31,32]:

$$(\boldsymbol{\sigma}_{eq}{}^2 / \boldsymbol{\sigma}_s{}^2) + 2q_1 f^* \cosh(-q_2\, p / 2\boldsymbol{\sigma}_s) - 1 - q_3 (f^*)^2 = 0 \tag{24}$$

where $\boldsymbol{\sigma}_s$ is the yield stress, q_1, q_2 and q_3 are model parameters, f^* is the parameter of material.

Parameter f^* was calculated by relations:

$$\begin{aligned} f^* &= f \;\; if \;\; f \le f_c \\ f^* &= f_c + (f_u - f_c) / (f_F - f_c) \;\; if \;\; f > f_c \end{aligned} \tag{25}$$

where f is the damage parameter, f_u = $[q_1+(q_1^2-q_3)^{1/2}]/q_3$, q_1, q_2, and q_3 are constants of the model, fc is the damage parameter at the beginning of nucleation damages, f_F is the damage parameter value corresponding to the final fracture of the material.

The model of damage process was used for determination of the damage parameter f [31,32].

$$\begin{aligned} \dot{f} &= \dot{f}_{nucl} + \dot{f}_{growth} \\ \dot{f}_{nucl} &= (f_N / s_N) \exp\{-0.5[\boldsymbol{\varepsilon}^p{}_{eq} - \boldsymbol{\varepsilon}_N) / s_N]^2\} \boldsymbol{\varepsilon}^p{}_{eq} \\ \dot{f}_{growth} &= (1-f)\dot{\boldsymbol{\varepsilon}}^p_{kk} \end{aligned} \tag{26}$$

where ε_N and s_N are the average nucleation strain and the standard deviation, respectively.

The model parameters of titanium alloys were determined throughout the numerical simulation of experimental stress-strain curves. Numerical values of model parameters were fitted by combined experimental and numerical techniques [38]. Numerical values of model parameters are given in Table 2.

Table 2 Dimensionless parameters for the GTN model for alpha titanium alloys.

Parameters of Eqs.(24)-(26)	q_1	q_2	q_3	f_0	f_N	fc	f_F	ε_N	s_N
Ti-5Al-2.5Sn (Grade 6)	1.3	1	1.69	0.00	0.2	0.035	0.4	0.28	0.1
Ti-6Al-4V (Grade 5)	1.5	1	2.25	0.00	0.02	0.023	0.145	0.35	0.1
Alpha Ti (Grade 2)	1.5	1	1.6	0.002	0.017	0.035	0.303	0.3	0.1

The friction shear stress $\boldsymbol{\tau}_{fr}$ in the contact interface between blocks is determined as [9]:

$$\boldsymbol{\tau}_{fr} = -\boldsymbol{\mu}(T)\frac{u_1}{|u_1|}p(x_i) \tag{27}$$

where $\boldsymbol{\tau}_{fr}$ is the friction shear stress, $\boldsymbol{\mu}(T)$ is the friction coefficient, u_1 is the particle velocity in sliding direction.

Fig. 2 shows the approximation temperature dependences of the friction coefficient and the thermal conductivity coefficient of titanium alloy.

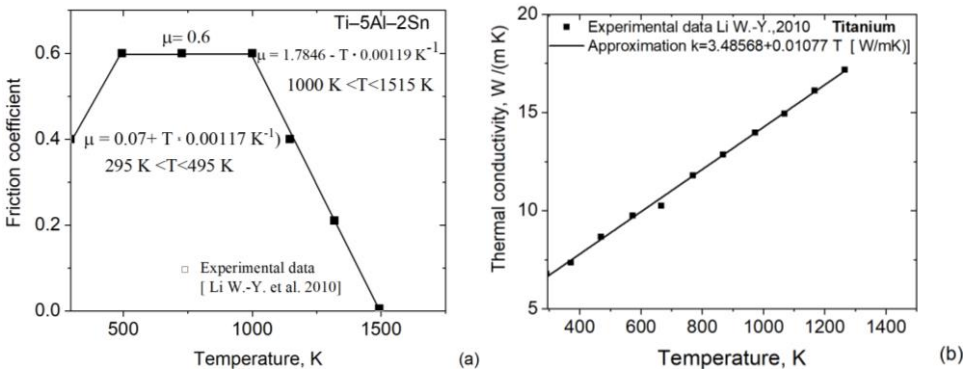

Fig. 2 Friction coefficient of titanium alloys versus temperature is shown in (a), the thermal conductivity coefficient versus temperature is shown in (b). Experimental data [8] are shown by symbols

The falling branch of the line in Fig. 2(a) reflects the decrease in the coefficient of friction of the alpha titanium alloy caused by the alpha-beta phase transition.

Experimental data on the coefficient of friction for titanium alloy Ti-5Al-2Sn correlate with data for alloy Ti-6Al-4V [39].

2.4 Boundary conditions

Boundary conditions corresponding to loading condition have the form:

$$
\begin{aligned}
&p\big|_{S_1} = p_{\,friction} \\
&u_i\big|_{S_1} = 0,\ i = 1,2,3 \\
&u_1\big|_{S_8} = V_0 \sin(\omega t) \\
&u_3\big|_{S_5} = 0 \\
&-\tau_{fr}\big|_{S_2} = \mu(T)\frac{u_1}{|u_1|}\,p(x_i) \\
&\sigma_{ij}\big|_{S_3 \cup S_4 S_6 \cup S_7 \cup S_8 \cup S_9 \cup S_{10} \cup S_{11} \cup S_{12} \cup S_{13}} = 0 \\
&T\big|_{S_1 \cup S_3 \cup S_4 \cup S_5 \cup S_6 \cup S_7 \cup S_8 \cup S_9 \cup S_{10} \cup S_{11} \cup S_{12} \cup S_{13}} = T_0
\end{aligned}
\tag{28}
$$

where $u_i \big|_{Sj}$ is the components of the particle velocity vector on the surface S_j, T_0 was assumed equal to 295 K.

The numbering of the surfaces Sj of the contacting blocks is shown in Fig. 1(a).

Initial conditions correspond to the free stress state of the material in a uniform temperature field.

3. Results of Numerical Simulation and Discussion

The formation of a strong weld joint of parts when using the technology of LFW is associated with the processes of diffusion and mass transfer at the boundary of the parts. Both of these processes are described using the used computational model. Fig. 2(a) shows the distribution of the effective plastic deformation near the friction surface, which is formed during the cyclic movement of the lower block. Obtained results indicate that the plastic flow of the near-surface layers of the block material is distributed inhomogeneously over the depth and area of the contacting blocks. The action of pressure in the contact zone of the blocks prevents the initiation of damage in the plastically deformable material, even when tensile stresses arise. Due to this, titanium alloys in the near-surface layers can be deformed in the regime of severe plastic deformation. The right tab in Fig. 2(b) shows the initial stage of material extrusion from the welding zone. The effect of extrusion of the titanium alloys during the LFW was recorded experimentally by Lachowicz [5], Li [8], Turner [37].

Extrusion of the alloy from the friction welding zone is caused by a pressure gradient and a significant decrease in the alloy flow stress as a result of heating. Fig. 2(b) demonstrates the calculated temperature distribution in the weld zone.

The simulation results indicate the deviation of the symmetry plane of the plastic deformation zone from the initial position of the contact plane of the blocks being welded (Fig. 2(b) left). This effect was discovered in recent experiments by Lachowicz [5].

This effect affects the flatness of welds, their mechanical properties and residual stress fields in the joints. The alpha (HCP) – beta (BCC) phase transition of titanium alloys upon heating in the LFW process lead to changing the mechanical properties of alloys. Therefore, the loading time LFW and the amount of accumulated plastic deformation have to be increased to obtain a welded joint.

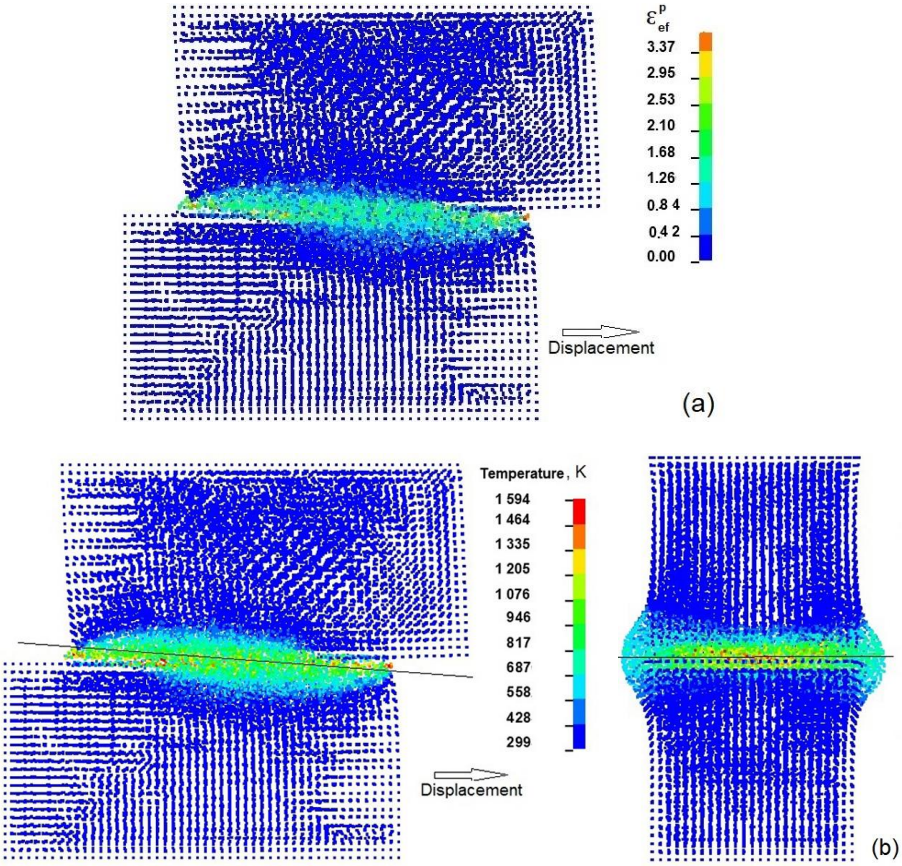

Fig. 2 The distribution calculated effective plastic strain in blocks during formation of LFW zone is shown in (a), distribution of temperature in the welded contact zone is shown in (b)

Fig. 3(a) shows the calculated field of equivalent stresses in the blocks at the time before the change in the direction of motion of lover block. The results explain the effect of stress on the flatness of the weld.

The presence of free surfaces S_3 and S_4 on the contact plane of the blocks (Fig. 1(a)) leads to a significant distortion of the spatial distribution of equivalent stresses, under the influence of which severe plastic deformations develop in the zone of formation of the weld. Note, that the specificity of LFW is that the distribution of equivalent stresses in the volume of the block being welded is not stationary, but depends on the frequency and amplitude of displacements. The contact area of the blocks also changes during cyclic movement.

The simulation results indicate that a complex stress state is realized in LFW zone. Fig. 3(b) shows the distribution of the Lode parameter characterizing the complex stress state. Thus, the simulation results confirm that for an adequate simulation of LFW process in metals and alloys, it is necessary to use plastic flow models in a complex stressed state.

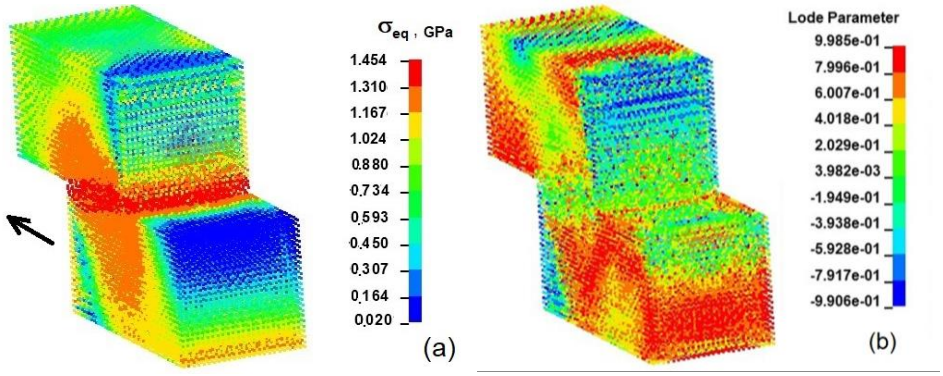

Fig. 3 Calculated equivalent stresses (von Mises stresses) upon contact of moving blocks in the process of LFW are shown in (a), calculated values of the Lode parameter (the triaxiality parameter of the stress state) at the contact of moving blocks in the process of LFW are shown in (b)

The unsteady field of equivalent stresses and the resulting rotation of the symmetry plane in the plastic flow zone of the contacting blocks contribute to the occurrence of localized material flows in the transverse direction relative to the movement of the blocks. Fig. 4(a) shows the calculated field of transverse displacements of the particles in the zone of formation of the weld. Fig. 2-4 shows the results obtained at velocity amplitude of 1000 mm/s.

The simulation results indicate the formation of vortices or rotational areas within the volume of plastically deformable material in the weld formation zone. Fig. 4(b) shows the movement of the particles of the material into the moving blocks along the normal to the plane of their contact (blue particles correspond to the upper block, red particles - to the lower block).

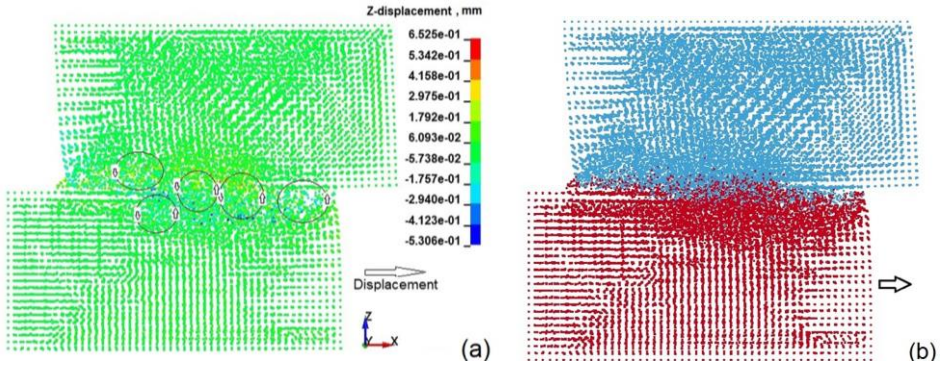

Fig. 4 Results of material particles transfer simulation in the LFW zone is shown in (a), displacements of mesoscopic particles of the particle material into moving blocks along the normal to the plane of their contact during LFW are shown in (b), (blue particles corresponds to upper block, red particles corresponds to low block)

The analysis of the evolution of the stress-strain state in the formation zone of the weld showed that the strain rates during cyclic loading vary over a wide range. Under the considered loading conditions, local strain rates reached 1000 s^{-1}. The results obtained confirmed the necessity of using wide-range constitutive equations for the numerical analysis of the process of LFW of titanium alloys.

In the LFW process, the temperature in the zone of strong plastic deformation of the titanium alloy can rise above the alpha-beta phase transition temperature $T_{\alpha\beta}$.

Note that the phase transition temperature $T_{\alpha\beta}$ for the titanium alloys discussed in this work can vary from 906 K to 923 K and depends on the concentration of chemical components that stabilize the beta phase. An increase in temperature is accompanied by a decrease in the plastic flow stress of the titanium alloy and the rate of heat release in the plastic deformation zone. In this regard, the question arises about the rational combination of the control parameters of LFW of titanium alloys to obtain strong joints.

Numerical simulation of the processes of LFW of different titanium alloys (Ti-5Al-2.5Sn (Grade 6), Ti-6Al-4V (Grade 5), alpha Ti (Grade 2)) under the same conditions showed that the laws of plastic flow of these alloys are qualitatively the same. Note that the quantitative differences in the values of the parameters of the stress-strain state and the distributions of temperature in the welded blocks from different titanium alloys confirm the need for an individual choice of LFW modes to obtain strong welded joints.

The condition for the specific power input parameter Q to exceed the critical value Q^* can be used as a criterion for the formation of a strong weld under LFW [9]:

$$Q = \frac{p u_{amp} \boldsymbol{\omega}}{2\pi S_{cont}} > Q^* \tag{20}$$

where $\boldsymbol{\omega}$ is frequency of displacement, u_{amp} is the amplitude of displacement, p is the pressure between welding parts, S_{cont} is the area of contact parts, Q^* is the parameter for one or a pair of materials to be welded.

The critical values of Q^* varies in the range from 5 up to 12 for titanium alloys [9]. The results of numerical simulation make it possible to assess the correctness of the choice of the control parameters of the process of LFW of three-dimensional structural elements made of titanium alloys to obtain a strong welded joint.

4. CONCLUSIONS

A new coupled thermomechanical 3D model of LFW process was used for studying the plastic deformation of joining structural elements from alpha and alpha + beta titanium alloys.

Numerical simulation of LFW thermomechanical process was carried by the SPH method. Calculations were performed using the LS DYNA software package (ANSYS WB 15.2) and the developed module for the constitutive equation.

The conclusions drawn from the numerical simulations are the following:

1) The formation of a welded joint occurs in a complex and unsteady stress-strain state.
2) In the near-surface layers of the bodies being welded, titanium alloys can be deformed in the mode of severe plastic deformation.

3) A deviation of the symmetry plane of the plastic deformation zone from the initial position of the contact plane of the bodies being welded occurs during a process of LFW.
4) Extrusion of material from the welded joint zone in the transverse direction with respect to the movement of bodies is caused by a pressure gradient and a decrease in the alloy flow stress due to heating.
5) The hcp−bcc phase transition of titanium alloys upon heating in the LFW process necessitates an increase in the cyclic loading time to obtain a welded joint.

Acknowledgement: *The work was supported by the Russian Science Foundation (RSF), project №20-79-00102. The authors would like to thank to the RSF.*

REFERENCES

1. Heidarzadeh, A., Mironov, S., Kaibyshev, R., Cam, G., Simar, A., Gerlich, A., Khodabakhshi, F., Mostafaei, A., Field, D.P., Robson, J.D., Deschamps, A., Withers, P. J., 2020, *Friction stir welding/processing of metals and alloys: A comprehensive review on microstructural evolution*, Progress in Materials Science, 100752.
2. Venu, B., BhavyaSwathi, I., Raju, L.S., Santhanam G., 2019, *A review on friction stir welding of various metals and its variable*, Materials Today: Proceedings, 18, Part 1, pp. 298-302.
3. Sai, S., Dhinakaran, M., Manoj, V., Kumar, K. P., Rajkumar, V., Stalin, B., Sathish, T., 2020, *A systematic review of effect of different welding process on mechanical properties of grade 5 titanium alloy*, Materials Today: Proceedings, 21, Part 1, pp. 948-953.
4. Gotawala, N., Shrivastava A., 2020, *Microstructural analysis and mechanical behavior of SS 304 and titanium joint from friction stir butt welding*, Materials Science & Engineering, A, 789, 139658.
5. Lachowicz, D.S., Bennett, C., Axinte, D.A., Lowth, S., Walpole, A., Hannon, C., 2021, *On the influence of tooling behaviour over axial shortening mechanisms in linear friction welding of titanium alloys and modelling plasticisation effects*, International Journal of Machine Tools and Manufacture, 161, 103674.
6. Ji, Y., Chai, Z., Zhao, D., Wu, S., 2014, *Linear friction welding of Ti–5Al–2Sn–2Zr–4Mo–4Cr alloy with dissimilar microstructure*, Journal of Materials Processing Technology, 214(4), pp. 979–987.
7. Okeke, S., Harrison, N., Tong, M., 2020, *Thermomechanical modelling for the linear friction welding process of Ni-based superalloy and verification*, Proceedings of the Institution of Mechanical Engineers, Part L: Journal of Materials: Design and Applications, 234(5), pp. 796-815.
8. Li, W.-Y., Ma, T., Li, J., 2010, *Numerical simulation of linear friction welding of titanium alloy: Effects of processing parameters*, Materials and Design, 31(3), pp. 1497–1507.
9. Vairis, A., Frost, M., 2000, *Modelling the linear friction welding of titanium blocks*, Materials Science and Engineering A, 292(1), pp. 8–17.
10. Su, Y., Li, W., Wang, X., Ma, T., Yang, X., Vairis, A., 2018, *On microstructure and property differences in a linear friction welded near-alpha titanium alloy joint*, Journal of Manufacturing Processes, 36, pp. 255–263.
11. Li, J., Shen, Y., Hou, W., Qi, Y., 2020, *Friction stir welding of Ti-6Al-4V alloy: Friction tool, microstructure, and mechanical properties*, Journal of Manufacturing Processes, 58, pp. 344–354.
12. Gangwar, K., Ramulu, M., 2018, *Friction stir welding of titanium alloys: A review*, Materials & Design, 141, pp. 230–255.
13. Lauro, A., 2012, *Friction stir welding of titanium alloys*, Welding International, 26(1), pp. 8–21.
14. Fall, A., Monajati, H., Khodabandeh, A., Fesharaki, M. H., Champliaud, H., Jahazi, M., 2019, *Local mechanical properties, microstructure, and microtexture in friction stir welded Ti-6Al-4V alloy*, Materials Science and Engineering A., 2019, pp. 166-175.
15. He, X., Gu, F., Ball, A., 2014, *A review of numerical analysis of friction stir welding*, Progress in Materials Science, 65, pp. 1-66.
16. Zhang, Z.; Tan, Z., 2019, *A multi scale strategy for simulation of microstructural evolutions in friction stir welding of duplex titanium alloy*, Journal High Temperature Materials and Processes, 38, pp.485-497.
17. Popov, V.L., Pohrt, R., Li, Q., 2017, *Strength of adhesive contacts: Influence of contact geometry and material gradients*, Friction, 5, pp. 308–325.

18. Chauhan, P., Jain, R., Pal, S.K., Singh S.B., 2018, *Modeling of defects in friction stir welding using coupled Eulerian and Lagrangian method*, Journal of Manufacturing Processes, 34, pp. 158–166.
19. Balokhonov, R., Romanova, V., Batukhtina, E., Sergeev, M., Emelianova, E., 2018, *A numerical study of the microscale plastic strain localization in friction stir weld zones*, Facta Univesitatis-Series Mechanical Engineering, 16(1), pp. 77-86.
20. Smolin, A.Y., Shilko, E.V., Astafurov, S.V., Kolubaev, E.A., Eremina, G.M., Psakhie, S.G., 2018, *Understanding the mechanisms of friction stir welding based on computer simulation using particles*, Defence Technology, 14(6), pp. 643-656.
21. Yan, F., Zhang, Y., Fu, X., Li, Q., Gao, J., 2019, *A new calculating method of frictional heat and its application during Friction Stir Welding*, Applied Thermal Engineering, 153, pp 250-263.
22. Rzaev, R., Dzhalmukhambetov, A., Chularis, A., Valisheva, A., 2019, *Mathematical modeling of process of the Friction Stir Welding*, Materials Today: Proceedings, 11, pp. 591–599.
23. Tartakovsky, A., Grant, G., Sun, X., Khaleel, M., 2006, *Modelling of Friction Stir Welding (FSW) process with smooth particle hydrodynamics (SPH)*, SAE Technical Paper Series, 01, 1394.
24. Tartakovsky, A.M., Meakin, P., 2005, *Modelling of surface tension and contact angles with smoothed particle hydrodynamics*, Physics Review E, 72, 026301.
25. Skripnyak, V.V., Skripnyak, V.A., 2020, *Fracture of titanium alloys at high strain rates and under stress triaxiality*, Metals, 10(3), 305.
26. Skripnyak, V.V., Kozulin, A.A., Skripnyak, V.A., 2019, *The influence of stress triaxiality on ductility of α titanium alloy in a wide range of strain rates*, Materials Physics and Mechanics, 42(4), pp. 415-422.
27. Sharkeev, Yu. P, Legostaeva, E.V., Vavilov, V.P., Skripnyak, V.A., Belyavskaya, O.A., Eroshenko A.Yu., Glukhov, I.A., Chulkov, A.A., Kozulin, A.A., Skripnyak, V.V., 2019, *Regular features of stage formation in the stress strain curves and microstructure in the zone of fracture of coarse-grained and ultrafine-grained titanium and zirconium alloys*, Russian Physics Journal, 62(8), pp. 1349-1356.
28. Sharkeev, Y., Vavilov, V., Skripnyak, V.A., Belyavskaya, O., Legostaeva, E., Kozulin, A., Chulkov, A., Sorokoletov, A., Skripnyak, V.V., Eroshenko, A., Kuimova, M., 2018, *Analyzing the deformation and fracture of bioinert titanium, zirconium and niobium alloys in different structural states by the use of infrared thermography*, Metals, 8(9), 703.
29. Skripnyak, V.V., Skripnyak, V.A., Skripnyak, E.G., 2019, *Fracture of titanium alloys at high strain rates and stress triaxiality*, Proc. 8th International Conference M2D-2019, Mechanics and Materials in Design, Bologna, pp. 81-82.
30. McAndrew, A.R., Colegrove, P.A., Flipo, B.C.D., Bühr, C., 2016, *3D modelling of Ti–6Al–4V linear friction welds*, Science and Technology of Welding and Joining, 22(6), pp. 496–504.
31. Neilsen, K.L., Tvergaard, V., 2010, *Ductile shear failure or plug failure of spot welds modelled by modified Gurson model*, Engineering Fracture Mechanics, 77, pp. 1031–1047.
32. Tvergaard, V., 2015, *Study of localization in a void-sheet under stress states near pure shear*, International Journal Solids and Structures, 60–61, pp. 28–34.
33. Shi, X., Zhao, C., Cao, Z., Zhang, T., Wang, T., Qiao, J., 2019, *Mechanical behavior of a near α titanium alloy under dynamic compression: Characterization and modeling*, Progress in Natural Science: Materials International, 29, pp. 432–439.
34. Donachie, M.J. Jr. *Titanium A technical guide*. Second Edition ASM Materials Park, Ohio, 2000.
35. Bros, H., Michel, M.-L., Castanet, R., 1994**,** *Enthalpy and heat capacity of titanium based alloys*, Journal of Thermal Analysis, 41, pp. 7–24.
36. Spigarelli, S., Ruano, O.A., El Mehtedi, M., del Valle, J.A., 2013, *High temperature deformation and microstructural instability in AZ31 magnesium alloy*, Materials Science and Engineering A, 570, pp. 135–148.
37. Turner, R., Gebelin, J.-C., Ward, R.M., Reed, R.C., 2011, *Linear friction welding of Ti–6Al–4V: Modelling and validation*, Acta Materialia, 59(10), pp. 3792–3803.
38. Springmann, M., Kuna, M., 2005, *Identification of material parameters of the Gurson–Tvergaard–Needleman model by combined experimental and numerical techniques*, Computational Material Science, 32, pp. 544–552.
39. Philip, J.T, Mathew J., Kuriachen B., 2019, *Tribology of Ti6Al4V: A review*, Friction, 7(6), pp. 497–536.